Experiments with a flow-through thermoacoustic refrigerator

R. S. Reid

Energy and Process Engineering Group, Los Alamos National Laboratory, Los Alamos, New Mexico 87545

G. W. Swift

Condensed Matter and Thermal Physics Group, Los Alamos National Laboratory, Los Alamos, New Mexico 87545

Deliberate superposition of steady flow parallel to the thermoacoustic oscillations in a stack is used to cool the steady flow as it passes through the stack. The loudspeaker-driven refrigerator described here cools a flowing helium–argon mixture from 35 to 27 °C and provides additional cooling power at a traditional cold heat exchanger. The dependence of the stack's temperature profile and of the additional cooling power on the steady flow rate are in agreement with a simple theory based on augmentation of the well-known thermoacoustic momentum, continuity, and energy equations with a single new term in the energy equation that describes the steady flow. © *2000 Acoustical Society of America.* [S0001-4966(00)04712-3]

PACS numbers: 43.35.Ud, 05.70.−a, 44.27.+g [SGK]

I. INTRODUCTION

The selection of technology for real-world applications depends on many factors, such as capital cost, operating cost, efficiency, size, weight, and reliability. Practical, economic considerations often favor technologies with nonoptimal efficiency. For example, the reverse Brayton-cycle refrigeration technology used aboard turbine aircraft provides weight savings that indirectly lead to lower aircraft operating cost, despite a cooling efficiency[1] that is less than 10% of the upper bound set by the laws of thermodynamics. The nascent technology of thermoacoustics seems attractive because the small number (often zero) of moving parts and sliding seals suggests low cost and reliability. Especially when both engine and refrigerator are present in one system, thermoacoustic devices are very simple: little more than heat exchangers of conventional design in large vessels that confine the thermoacoustic working gas and define the geometry in which the gas resonates.

In an attempt to enhance this inherent simplicity, we have begun to explore whether some of the heat exchangers can be eliminated from thermoacoustic devices. Figure 1 illustrates the idea for a thermoacoustic refrigerator used to cool air. Figure 1(a) shows the main parts of an air-conditioning system using a conventional standing-wave thermoacoustic refrigerator. In addition to the stack, four heat exchangers are required: two in the thermoacoustic working gas and one in each of the two air streams. Heat transfer between the working-gas heat exchangers and the air heat exchangers, indicated by heavy black arrows, is accomplished via heat-transfer loops such as pumped water, heat pipes, thermosyphons, etc. In mass production, the four heat exchangers and two heat-transfer loops would probably account for most of the capital cost of this system.

The air-conditioning system in Fig. 1(b) illustrates the simplification that is possible by using the indoor air itself as the thermoacoustic gas. A midwall in the indoor-air duct separates two acoustic resonators, driven 180° out of phase from each other by an oscillating driver piston in the center of the midwall. The drive frequency is chosen to make the acoustic wavelength equal to twice the midwall length, so pressure nodes will be at the ends of the midwall and, hence, negligible acoustic power will be radiated to distant parts of the duct. The position of the stack relative to the nodal pattern of the standing wave is chosen so that conventional standing-wave thermoacoustic phenomena pump heat from right to left. Superimposed on these thermoacoustic phenomena, the air is forced slowly rightward through the stack from ambient to cold, so that cold air leaves the right end of the apparatus. Compared to Fig. 1(a), two heat exchangers are eliminated, suggesting a reduction in capital cost.

This intimate superposition of steady flow of the air with its own oscillating thermoacoustic flow might also give the system of Fig. 1(b) a higher efficiency than that of the system of Fig. 1(a), for two reasons. First, the internal temperature differences of two heat exchangers are eliminated and the acoustic power dissipation in the missing thermoacoustic heat exchanger is eliminated. Second, a much more subtle yet significant improvement in efficiency can occur because the system of Fig. 1(b) puts the air stream sequentially in thermal contact with a large number of refrigerators in series—a continuum limit of staged refrigerators. To understand this point, imagine that thermoacoustic refrigerators were ideal, having Carnot's coefficient of performance $T_C/(T_0−T_C)$, where T is temperature and the subscripts C and 0 represent cold and ambient. Then, in the case of Fig. 1(a), the removal of heat $\dot{m}c_p(T_0−T_C)$ from the air stream with mass flow rate $\dot{m}$ and isobaric specific heat c_p by the refrigerator's cold heat exchanger at temperature T_C would require that work

$$\dot{W}=\dot{m}c_p(T_0−T_C)^2/T_C \tag{1}$$

must be supplied to the refrigerator by the driver piston. This is more than twice the minimum work required by the first and second laws of thermodynamics for this process, which is given by the difference between the outgoing and incoming flow availabilities,[2]
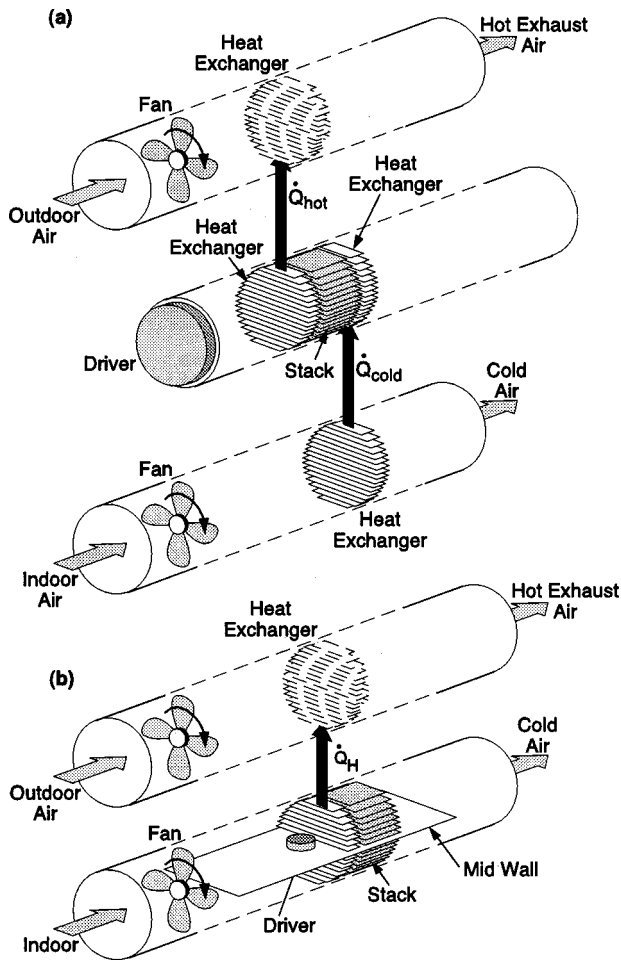
FIG. 1. An air conditioner is used to illustrate the potential simplification of hardware that is possible if the process gas is used as the thermoacoustic working gas and parallel steady flow is superimposed on the thermoacoustic oscillations. The air-conditioning system must remove heat from a stream of indoor air (the ''process gas'') and reject waste heat to a stream of outdoor air. (a) A conventional thermoacoustic air-conditioning system would require four heat exchangers and two heat-transfer loops in addition to the stack. (b) By using the indoor air itself as the thermoacoustic working gas and superimposing steady flow on the oscillating flow, two heat exchangers and one heat-transfer loop are eliminated.

$$\dot{W} = \dot{m}[(h_C - h_0) - T_0(s_C - s_0)] \tag{2}$$

$$= \dot{m}c_p[T_C - T_0 + T_0\ln(T_0/T_C)], \tag{3}$$

where h is enthalpy per unit mass and s is entropy per unit mass. [Equation (3) results from using ideal-gas expressions for h and s.] The lower efficiency of the simple refrigerator of Fig. 1(a) occurs because it removes *all* the heat from the air stream at T_C, where every unit of cooling power requires $(T_0 - T_C)/T_C$ units of input power. It is more efficient to remove as much of the heat load as possible at higher temperatures T_C', where $T_0 > T_C' > T_C$, so that each unit of cooling power requires only $(T_0 - T_C')/T_C'$ units of input power. The flow-through thermoacoustic refrigerator of Fig. 1(b) is an imperfect embodiment of this idea, with each differential length dx of the stack essentially a tiny refrigerator unto itself, lifting heat from T_C' to $T_C' + dT_C'$, removing each unit of heat from the flowing air stream at the highest possible temperature.
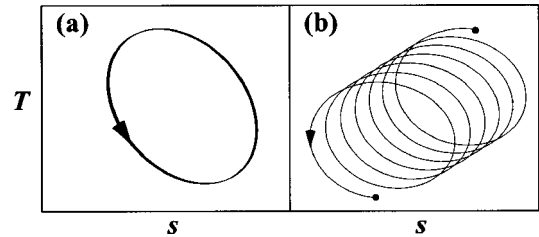
FIG. 2. When $\dot{m} = 0$, a typical parcel of gas in a thermoacoustic stack follows one elliptical temperature–entropy ($T-s$) cycle repeatedly, as shown schematically in (a). When $\dot{m} \neq 0$, a given parcel of gas follows a much more complicated path through $T-s$ space, as shown schematically in (b).

With the addition of a small nonzero steady flow along x, the air moves through the stack in a repetitive, ''51 steps forward, 49 steps back'' manner in position, and also in temperature, density, and entropy as illustrated in Fig. 2(b). This violates one assumption on which most prior thermoacoustic equations[3–5] are based—that the x component of gas velocity is given by $u = \text{Re}[u_1 e^{i\omega t}]$, with zero average value. (The subscript 1 indicates a complex amplitude.) However, the derivation of corresponding thermoacoustic equations in the presence of nonzero steady flow is straightforward.[6,7] The thermoacoustic momentum, continuity, and wave equations are unchanged to lowest order, but the steady flow appears in the thermoacoustic energy equation, which becomes

$$\dot{H}_2 = \dot{m}c_p(T_m - T_0) + \tfrac{1}{2}\rho_m c_p$$

$$\times \int \text{Re}[T_1 \widetilde{u_1}] dA - (Ak + A_{\text{solid}}k_{\text{solid}})\frac{dT_m}{dx} \tag{4}$$

for an ideal gas. The subscript m indicates the local mean value, $\dot{H}_2$ is the total energy flow in the x direction, A is the cross-sectional area in the stack that is available to the gas, k is the thermal conductivity of the gas, and k_{solid} is the thermal conductivity of the stack walls. The complex temperature oscillation amplitude T_1 can be expressed in terms of pressure and velocity amplitudes p_1 and u_1. In Eq. (4), the new, first term represents enthalpy carried by the steady flow, the familiar[4] second term represents enthalpy carried by the oscillating flow, and the third term represents ordinary conduction of heat down the temperature gradient in the gas and solid. Note that the second term is second order in the acoustic oscillation amplitude, so this equation will be most interesting and valid when the steady flow $\dot{m}$ is smaller than or roughly comparable to a second-order mass flow such as $A|\rho_1||u_1|$, where ρ is gas density; hence, we retain the traditional subscript ''2'' on $\dot{H}_2$. This bound on $\dot{m}$ also ensures that the steady flow is always in excellent local thermal contact with the stack channel walls, as long as these walls are separated by no more than several thermal penetration depths.

For the usual situation in which the stack is laterally thermally insulated, energy conservation requires that $\dot{H}_2$ is independent of x. Hence, if p_1 and u_1 are known, Eq. (4) can be used as a differential equation for $T_m(x)$ to predict the temperature profile in the stack. Numerical integration of this differential equation, self-consistently with the momentum and continuity equations, is straightforward.[8] However,

qualitative insight about the temperature profile can be obtained more easily by making some approximations. Several sets of approximations are plausible, but all lead to qualititatively similar results;[6,9] here, we choose a mathematically simple set of approximations. Following the inviscid boundary-layer ''short-stack'' approximation,[5] suppose that the stack is short enough and spans a small enough temperature difference that thermophysical properties and sound-wave properties can be regarded as independent of x to lowest order, and suppose that the ordinary conduction of heat down the temperature gradient is small. Then Eq. (4) reduces to

$$\dot{H}_2 = \dot{m}c_p(T_m - T_0) + \frac{1}{4}A\frac{\delta_\kappa}{r_h}|p_1||u_1|\left(\frac{dT_m/dx}{\nabla T_{\text{crit}}} - 1\right), \quad (5)$$

where δ_κ is the thermal penetration depth, r_h is the hydraulic radius of the pores in the stack, and $\nabla T_{\text{crit}} = -\omega|p_1|/\rho_m c_p|u_1|$. Treating everything except the two explicit occurrences of T_m in Eq. (5) as independent of x and setting $d\dot{H}_2/dx = 0$ yields

$$\frac{T_0(x) - T_m(x)}{T_0 - T_C} = \frac{1 - e^{-\Xi x}}{1 - e^{-\Xi L}}, \quad (6)$$

where L is the length of the stack and

$$\Xi = \frac{4\dot{m}c_p\nabla T_{\text{crit}}}{A|p_1||u_1|\delta_\kappa/r_h}. \quad (7)$$

In this approximation, Eq. (5) shows that $T_m(x)$ is linear when $\dot{m} = 0$. For nonzero $\dot{m}$, Eq. (6) shows that $T_m(x)$ is exponential, with characteristic length $1/\Xi$, so that the curvature increases with increasing $|\dot{m}|$ and the sign of the curvature depends on the sign of $\dot{m}$.

The elimination of heat exchangers by superimposing parallel steady flow and thermoacoustic oscillation should be possible in engines as well, but we chose to investigate this idea in the context of a refrigerator. The next section describes the apparatus, topologically similar to that illustrated in Fig. 1(b). In this first exploration of the idea of superimposed parallel steady flow and of Eq. (4), we had no reason to demonstrate a practical device, so we used ordinary inefficient loudspeakers to drive the acoustic resonance, in what roughly resembles a full-wavelength torus with side branches for injection and removal of steady flow. Our primary intent was the verification of the qualitative features of Eq. (6), so the stacks were equipped with many thermocouples to measure $T_m(x)$. Power-measuring instrumentation was also included, to investigate Eq. (4) more directly. In the course of the measurements, it was easy to change the direction of $\dot{m}$, so we did this, to expand the range of these investigations, creating a type of steady-flow heat pump as $\dot{m}$ flowed up the temperature gradient. The results of these investigations, described in the final section, provide qualitative and quantitative confirmation of the ideas presented in this introduction. A more complete description of the ideas, the experiment, and the analysis is available elsewhere.[6]
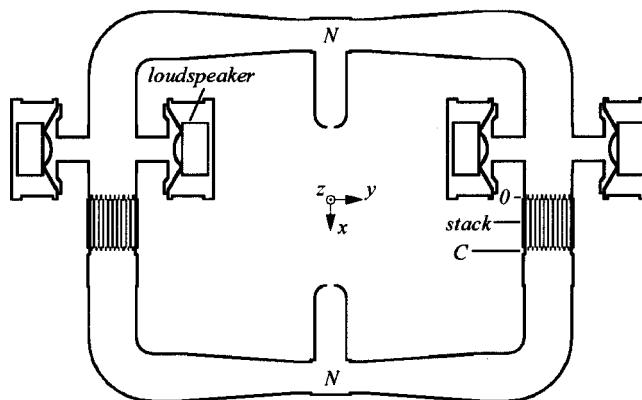

FIG. 3. Schematic of the experimental apparatus, with internal resonator dimensions drawn to scale. Spacings between plates in the stacks and heat exchangers are not to scale. The apparatus is left–right symmetric. The heat exchangers at T_0 and T_C are indicated by ''0'' and ''C.''

II. APPARATUS AND INSTRUMENTS

A schematic of the apparatus built for these investigations is shown in Fig. 3, with internal dimensions drawn to scale. The toroidal resonator had a total internal volume of 0.0915 m³ filled with a mixture of 92% helium and 8% argon at 3.23-bar mean pressure. (The system was also successfully operated with atmospheric air, but the helium–argon mixture provided larger, more accurately measurable powers.) Four speakers drove the fundamental gas resonance, with the speaker pair on one side of the resonator moving out of phase from the speaker pair on the other side. The two pressure nodes of the standing wave (marked ''N'') divided the resonator into symmetric left and right halves and provided convenient locations for injection and removal of steady flow. The stacks and their heat exchangers were positioned in the standing wave so that $|p_1|/\rho_m a|u_1| \simeq 1.5$ in mid stack, where a is the sound speed. Although this location generated significant viscous losses, it lowered the temperature gradient so that thermal conduction losses were negligible. For convective stability under normal operating conditions, the apparatus was oriented as shown in the figure, with the ambient ends of the stacks up.

The resonator was made of polyvinyl-chloride pipe and fittings, aluminum housings containing the speakers, and a few other custom-fabricated parts, sealed together with glue or bolted rubber gaskets. The four long conical diffusers reduced harmonic content[10] in the standing wave to negligible levels. Dynamic pressure sensors[11] at six locations in the resonator were used to verify that the pressure nodes were indeed nodes and that the wave shape was as expected. The amplitudes and phases of the oscillating pressures, here and elsewhere, were measured with a dynamic signal analyzer,[12] and sometimes checked with a lock-in amplifier. The 94-Hz fundamental resonance frequency measured at low amplitude in the resonator when filled with commercially procured mixed gas agreed within 0.5 Hz with similar measurements using our own mixtures made from pure helium and argon, indicating that the commercial and home-made helium fractions agreed within 0.2%. The measured frequency also agreed within 1 Hz with the value calculated using a DeltaE[8] model of the complete apparatus with as-built dimensions,

and the low-amplitude quality factor (measured by sweeping frequency) agreed within a few percent with the calculated value, helping to build our confidence in this numerical model.

Each stack consisted of 142 parallel, 0.25-mm-thick fiberglass plates with length 15.24 cm along the acoustic-oscillation direction, contained in a 15.32-cm-i.d. polyvinyl-chloride resonator pipe. The separation between plates was 0.81 mm, maintained by straight lengths of epoxy-coated nylon monofilament, aligned along the acoustic-oscillation direction, and located on 13.5-mm centers. Thus, 70% of the pipe's cross-sectional area was open to gas flow, through many channels 15.24 cm long, each with a rectangular cross section 0.81 mm high by 12.7 mm wide, except near the circumference of the stack where the circular package perimeter truncated the width of many channels. The separation between plates was about two thermal penetration depths of the helium–argon mixture at the operating conditions. Fiberglass and nylon were used to minimize heat conduction along the stack plate in the direction of sound propagation. The stack length was much less than the radian length of the sound wave but many times larger than the oscillatory gas displacements. The fabrication of these stacks is described fully in Ref. 6.

Five 3.2-mm-diameter fiberglass support tubes, extending along the stack diameter, perpendicular to the plates, with 2.54-cm center-to-center spacings, guided 0.5-mm-diameter sheathed copper–constantan thermocouples[13] with ''special limits of error'' into the stack. The junctions of ten thermocouples were epoxied to one plate's surface at ten axially equally spaced positions along the full 15.24-cm length of the rectangular channel at the center of the stack. The thermocouples were attached to the plate 3 mm to one side of the fiberglass support tubes. The channel containing the thermocouples was blocked at each end to eliminate thermoacoustic effects on the thermocouple sheaths and wires in that channel. Thus, the temperature measured was produced primarily by thermoacoustic effects in the adjacent, unblocked channels.

Adjacent to and above each stack was a water-cooled, ambient-temperature heat exchanger used to transfer waste heat from the refrigerator to the ambient environment. This exchanger extended 1.27 cm along the acoustic-oscillation direction. Rubber O-rings sealed its case to the stack's pipe below and to another polyvinyl-chloride pipe above. The exchanger's single bank of eight 0.48-cm-o.d. copper tubes were soft-soldered into its 14.8-cm-i.d. brass case and to its 80 copper fins, which had 0.53-mm thicknesses and 1.27-mm separations. A copper–constantan thermocouple measured the temperature of one of the copper fins. A total of 90 cm^2 (52% of the case inside area) was open to oscillating gas. The thermal resistance measured between the copper tubes and the water flowing through them was 77 °C/kW; the thermal resistance from the middle of each fin to its nearby tubes was calculated to be 3.4 °C/kW.

Manifolds connected the tubes at the inlet and outlet of the ambient exchanger. A copper–constantan thermocouple immersed in the water inside each manifold measured the water temperature entering or leaving the exchanger. The water flow rate to the exchanger was measured with a variable-area rotameter. The heat rejection rate from the exchanger was calculated from the flow rate and manifold temperature measurements. Uncertainty in the calculated heat-rejection rate was typically less than ±10% of reading, but was a strong function of thermoacoustic conditions and water flow rate.

Other heat exchangers were placed at the cold ends of the two stacks. These electrically heated ''cold'' heat exchangers were unnecessary for cooling the steady flow of gas, but they allowed versatile measurements and control in the experiments. For example, by using these heat exchangers to hold the stack ends at constant temperature while steady flow was varied, the only temperature equilibration required was inside the stacks, so equilibration time was minimized and system resonance frequency stayed constant. Each cold heat exchanger consisted of a continuous nichrome ribbon, 50.8-μm thick and 6.35-mm wide, supported by a fiberglass frame to form a back-and-forth grid. The room-temperature electrical resistance of the ribbon was about 30 Ω. Power from voltage-controlled alternating electric current was dissipated in the nichrome ribbon. A digital multimeter detected root-mean-square (rms) voltage across the ribbon; a thermocouple near the center of the exchanger's fiberglass frame monitored the local temperature.

The four speakers[14] used to drive the resonator were well suited to this low-cost proof-of-principle experiment. Speaker pairs were contained in machined and welded aluminum housings with penetrations for electrical power and cooling water. These speakers were factory-equipped with a cooling system, in which motion of the diaphragm caused high-velocity gas motion around the voice coil and through three ports in the magnet. Nevertheless, additional cooling was needed to keep the voice coils at acceptable temperatures during typical operation, so a small plate was added to the rear of each speaker's magnet to form a small sealed chamber, and water was circulated through this chamber. The temperatures of the entering and exiting flows were measured with chromel–alumel thermocouples, and a variable-area rotameter indicated the water flow rate through each speaker chamber, so that heat removal from the speakers could be determined.

The properties of each speaker were characterized by measuring Bl product, mechanical resistance, electrical resistance, voice-coil inductance, and diaphragm stiffness. The Bl product of each speaker was measured by applying increasing amounts of weight to the speaker diaphragm and increasing the direct current applied to the voice coil while keeping the diaphragm stationary. Mechanical properties were found by measuring the electromechanical resonance frequency with the speaker in vacuum, and simply using the manufacturer's supplied data for the mass of the moving diaphragm. Strong temperature dependence was noted in diaphragm stiffness, so these measurements were taken at several temperatures to characterize this dependence. The inductance was found by epoxying the voice coil of one speaker to its magnet to prevent motion and measuring the electrical resonance frequency with the voice coil in series with a known capacitance.

The mechanical spring constant and moving mass were small enough, and the associated mechanical resonance frequency was close enough to 94 Hz, that the impedance of the speakers was small compared to that of the acoustic standing wave in the gas, and the pressure amplitude in the cavity behind each speaker was nearly equal to the pressure amplitude just in front of the speaker. This design[15] places such a power transducer at an optimal location in the standing wave, neither at a pressure node nor at a velocity node, and allows the pressure difference across the speaker to be due only to the power delivered to the wave by the speaker. The four speakers were driven by a single sinusoidal function generator with variable frequency and amplitude, through four adjustable ''microphone mixers,'' each feeding a power amplifier. The mixers were set so that the four speakers produced nearly equal acoustic powers, thereby accomodating minor differences in Bl product among the speakers. The electrical power supplied to each speaker was obtained with a dynamic signal analyzer,[12] which measured the voltage across the speaker terminals, the voltage across a precision, temperature-controlled current-sensing resistor in series with the speaker, and the phase between these voltages.

Accelerometers attached to speaker diaphragms have been used previously[16] to measure the volume velocity so that the acoustic power delivered by the speaker can be determined. A simpler method to measure volume velocity was attempted in this experiment, requiring only measurement of $p_{1,\text{back}}$ in the cavity behind the speaker's diaphragm using a piezoresistive pressure transducer. Assuming adiabatic oscillations in the cavity volume V_{back}, the complex volume velocity U_1 of the diaphragm is

$$U_1 = -\frac{i\omega V_{\text{back}}}{\gamma p_m} p_{1,\text{back}},\tag{8}$$

with the signs chosen so that positive volume velocity flows into the resonator from the front of the diaphragm. The time-averaged acoustic power transferred to the resonator by the front of the speaker is then

$$\dot{W}_{ac} = \frac{\omega V_{\text{back}}}{2\gamma p_m} \text{Im}[p_{1,\text{back}}\tilde{p}_{1,\text{front}}].\tag{9}$$

Correcting this expression to account for laminar thermal-relaxation effects on the surface area A_{back} of the cavity behind the speaker leads[17,18] to a factor $1-i(\gamma-1)A_{\text{back}}\delta_\kappa/2V_{\text{back}}$ inside the square bracket of Eq. (9), but this is negligible here.

Calculating acoustic power delivered to the resonator using Eq. (9) requires knowledge of the volume V_{back} behind the speaker diaphragm. This volume was estimated using fabrication drawings of the speaker housing, measuring the speaker frame's volumetric displacement in water, and accounting for the volume occupied by cooling lines and other minor irregularities. The volume behind each speaker diaphragm was estimated to be 7.9×10^{-3} m^3 $\pm4\%$. Including uncertainties in pressure measurements, the result obtained from Eq. (9) was typically uncertain by $\pm8\%$.

The deliberate steady flow was delivered to and removed from the resonator at the two pressure nodes, so that the connections to the steady-flow pumping system did not perturb the resonance or absorb significant acoustic power. Two compressors[19] in series, with water-cooled heat exchangers downstream of each, circulated the steady flow of the helium–argon mixture through the resonator. The gas flow rate was controlled by throttling the flow to the suction side of the first compressor and by allowing some of the gas discharged by the second compressor to return to the suction side of the first compressor through a bypass. An expansion chamber between this compressor assembly and the resonator, together with the inertance of the connecting tubing, acted as a low-pass acoustic filter to keep velocity and pressure oscillations generated by the compressor assembly out of the resonator. The sign of the gas flow through the resonator could be reversed by interchanging the connections between the compressor assembly and the resonator.

Before entering the resonator, the steady flow passed through a filter to remove dust and then through a laminar flow resistance.[20] The differential pressure that formed across the laminar flow resistance as gas flowed through it caused a pressure difference proportional to flow rate. The flow resistance was calibrated by the manufacturer using a NIST-traceable ANSI Z540-1 standard. After months of preliminary experiments, just before the measurements discussed in detail below were made, the flow resistance was returned to the manufacturer for recalibration and was found to be within tolerance. Two redundant piezoresistive pressure transducers[11] detected the differential pressure across this resistance. The transducers were calibrated at 323-kPa mean pressure using a water manometer. The mass flow rate $\dot{m}$ through each stack was found by correcting for absolute temperature and pressure and assuming that the flow was evenly divided between resonator sides. The uncertainty in $\dot{m}$ was estimated to range from $\pm3\%$ at the lowest flow rate, where uncertainty in the temperature correction dominated, to $\pm0.9\%$ at the highest flow rate, where the uncertainty in the calibrated flow resistance was most important.

Stationary thermocouples near the pressure nodes and movable thermocouples above and below the stack–heat-exchanger assemblies detected temperatures in the moving gas; the tips of these sheathed thermocouples were oriented perpendicular to the oscillating flow to minimize measurement error from thermoacoustic heat pumping along the sheaths.

To thermally insulate the refrigerator from the room, the entire resonator/speaker system was suspended by nylon rope inside a large box filled with 10-mm-diameter polystyrene packing beads. Instrument cables, power leads, and water lines entered through the open top of the box. The efficacy of this insulating method was revealed in comparisons of the total electrical power dissipation with the total thermal power carried by the water cooling lines and steady-flow circuit. When the refrigerator was allowed to operate long enough (typically 6 h) to reach equilibrium, the fractional difference between the heat rejected to the water and the algebraic sum of the other powers was typically less than 3%.

III. RESULTS

As $\dot{m}$ was varied during measurements, the values of $|p_1|$, T_0, and T_C were held constant by adjusting the electric power to the speakers, the water flow rate through the ambient heat exchanger, and the electric power $\dot{Q}_C$ supplied to the cold heat exchanger. This resulted in a condition that also kept resonator temperature constant, so the resonance frequency was fixed. The effects of $\dot{m}$ on the dependent variables $T_m(x)$, $\dot{W}_{ac}$, and $\dot{Q}_C$ were then measured. We selected $|p_1|/p_m = 0.020$ as a reasonable compromise between power (more accurately measurable at higher amplitudes) and consistency with the low-amplitude approximation inherent in thermoacoustic analysis based on Rott's work.[3,4] We selected $T_0 = 308.0$ and $T_C = 300.5$ K; this temperature difference was large enough for accurate temperature measurements yet small enough that the refrigerator could provide a large, accurately measurable cooling power.

Although a complete numerical model (described in Ref. 6) of the entire apparatus was used for some comparisons, the most important numerical results were obtained with a much simpler partial model that integrated[8] from the pressure node at the bottom of the resonator up through one stack–heat-exchanger assembly just to the location of the pressure sensor above the stack–heat-exchanger assembly. Thus, uncertainty about speaker power (see below) did not affect the results of this integration. The usual thermoacoustic momentum and continuity equations were integrated throughout the model, and were augmented in the stack by Eq. (4). The geometry, the gas pressure and mixture composition, the operating frequency, the temperatures at the two ends of the stack, the steady mass flow rate, the pressure amplitude at the pressure transducer above the stack–heat-exchanger assembly, and $p_1 = 0$ at the pressure node were set equal to their experimental values and treated by the integration as given. Results of the integration then included the complex pressure and volume velocity everywhere, the temperature profile within the stack, the cooling load applied at the cold heat exchanger, and the acoustic power supplied at the top of the stack–heat-exchanger assembly.

The dramatic effect of $\dot{m}$ on $T_m(x)$ is illustrated in Fig. 4, which shows the temperature as a function of distance from the ambient end of the stacks for a few representative values of $\dot{m}$. The filled and open symbols represent the measured values, with the error bars showing the uncertainties in the thermocouple readings. At $\dot{m} = 0$ the temperature profile is nearly linear, as discussed in the Introduction. Nonzero $\dot{m}$ distorts the temperature profile with sign and shape consistent with the qualitative description in the Introduction and the approximate Eq. (6). The similarity between Figs. 4(a) and (b) also shows that the steady flow is substantially equal in the two stacks, although the steady-flow delivery system guarantees only that the sum of the flow rates through the two stacks is fixed. The fact that the steady flow always automatically split evenly between the two stacks is encouraging for possible practical applications; we had no *a priori* reason to be certain of such stability.

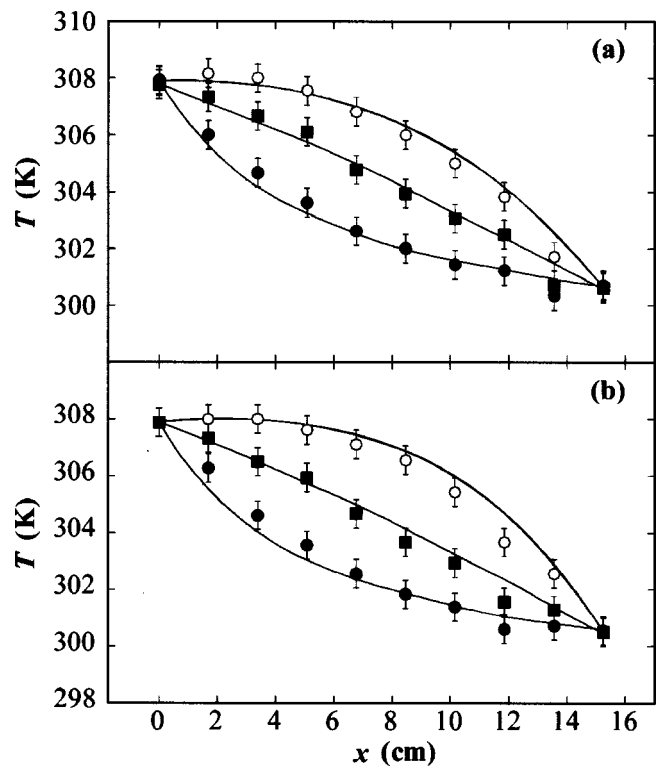The solid curves in the figure represent numerical

FIG. 4. Mean temperature as a function of distance from the ambient end of the stack, at representative steady flow rates. (a) Left stack. Squares, $\dot{m} = 0$; open circles, $\dot{m} = 3.35$ g/s; filled circles, $\dot{m} = -4.34$ g/s. (b) Right stack. Squares, $\dot{m} = 0$; open circles, $\dot{m} = 4.51$ g/s; filled circles, $\dot{m} = -4.34$ g/s. The curves are the results of numerical integrations of Eq. (4) and the thermoacoustic momentum and continuity equations.

integration[8] of the partial model described above, incorporating Eq. (4). Overall, the measurements and numerical integrations of $T_m(x)$ are in good agreement, confirming the understanding of superimposed thermoacoustic and steady flow embodied in Eq. (4). It is difficult to provide quantitative estimates for the uncertainty in the calculated curves, which could be due to uncertainties in fabricated geometry (such as the presence of the fiberglass stack supports, slightly nonparallel nylon-monofilament stack spacers, etc.) and to the low-amplitude acoustic model's assumption that the gas displacement amplitude is much smaller than the stack length (see below).

Obtaining the experimental power $\dot{Q}_C$ absorbed by the stack from the cold heat exchanger required some care, because some of the electric power $\dot{Q}_{elec}$ dissipated in the cold heat exchanger was transferred to the steady flow, causing a small difference between the temperature T_C of the cold end of the stack and the time-averaged temperature of the gas just below the heat exchanger, T_{below}. The heat load absorbed by the cold end of the stack was obtained from $\dot{Q}_{elec}$ by measuring these two temperatures and using

$$\dot{Q}_C = \dot{Q}_{elec} - \dot{m} c_p (T_{below} - T_C). \tag{10}$$

This steady-flow correction for obtaining $\dot{Q}_C$ was, of course, zero at $\dot{m} = 0$. It was largest for the largest $\dot{m}$ and smallest $\dot{Q}_C$, where for example $\dot{Q}_C = 3$ W and $\dot{Q}_{elec} = 19$ W for $\dot{m} = 3.5$ g/s for the left stack. At the opposite extreme for the
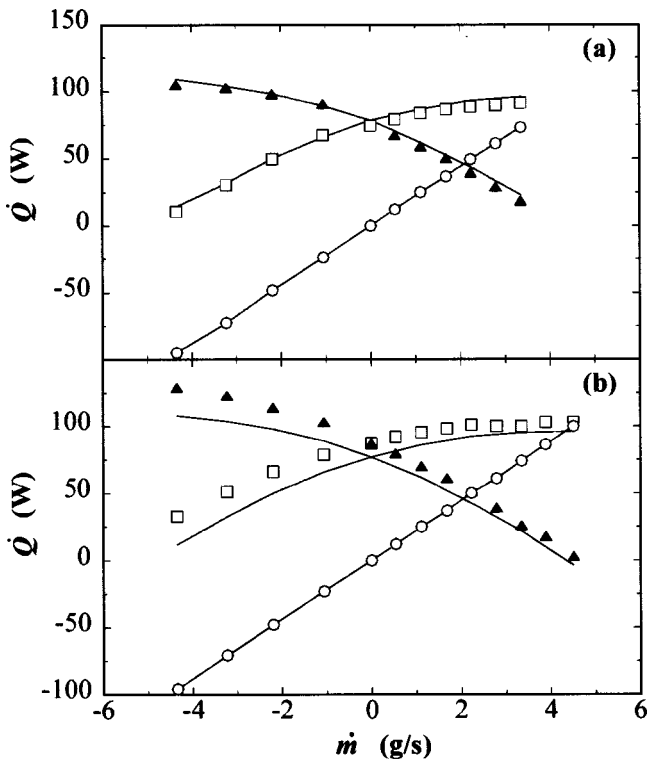
FIG. 5. Several thermal powers $\dot{Q}$ as a function of steady flow rate $\dot{m}$, (a) for left stack and (b) for right stack. Symbols are experimental results and lines are numerical results. The circles are steady-flow enthalpy change, the triangles are the heat $\dot{Q}_C$ extracted from the cold heat exchanger by the stack, and the squares are the sum of these two. (At $\dot{m}>0$, the curves end where $\dot{Q}_C$ drops to zero.)

left stack, $\dot{Q}_C = 129$ W and $\dot{Q}_{\text{elec}} = 100$ W for $\dot{m} = -4.2$ g/s.

Figure 5 shows some powers as a function of steady mass flow rate, all at $|p_1|/p_m = 0.020$, $T_0 = 308.0$ K, and $T_C = 300.5$ K. Signs for all $\dot{Q}$'s and for $\dot{m}$ are chosen so that positive values correspond to operation as a refrigerator: Positive heat transfer rates flow into the stack, removing heat from the steady flow or from the cold heat exchanger. Symbols are measured values, with the uncertainties in the data typically lying within the areas covered by the symbols. The curves are the results of numerical integrations of the partial model.

The open circles and associated straight lines are simply $\dot{m}c_p(T_0 - T_C)$, representing the enthalpy removed from the steady flow as it passed through the stack. The dark triangles are cold-end cooling powers $\dot{Q}_C$, obtained from measured values of electric power dissipation in the cold heat exchanger and corrected for steady flow using Eq. (10). The open squares represent the total refrigeration power: the sum of $\dot{Q}_C$ and the steady flow's enthalpy change across the stack. The curves associated with the triangles and squares are numerical integrations of the relevant equations, obtained in the same fashion as the curves in Fig. 4.

The qualitative trends in the observed dependences of $\dot{Q}_C$ and $\dot{Q}_C + \dot{m}c_p(T_0 - T_C)$ on $\dot{m}$ are predicted very well by the numerical integrations of Eq. (4) and the other thermoacoustic equations, reinforcing our confidence in Eq. (4).
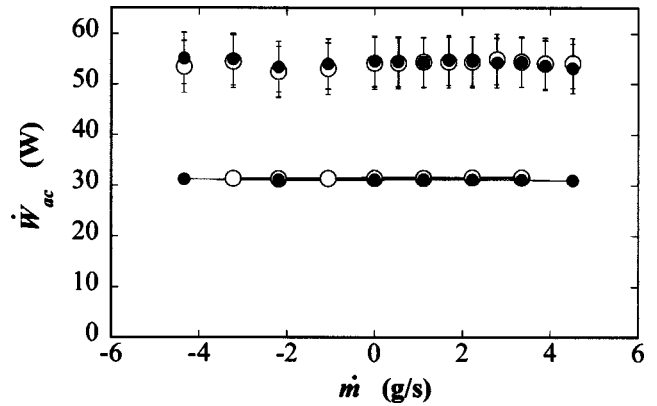

FIG. 6. Acoustic power delivered by the speakers as a function of steady flow rate. Open symbols are for the left speaker pair, and filled symbols for the right speaker pair. The values near 55 W are the result of Eq. (9), using experimental values for pressure amplitudes obtained during the measurements described in Sec. II. The values near 33 W are the result of a DeltaE model, using the speaker parameters obtained during preliminary measurements described in Sec. I.

Quantitative disagreements between the measurements and numerical integrations are less than 20 W, typically 10% of total power, and are probably due to a combination of uncertainty in geometrical parameters of the hardware that are used in the numerical integration and inappropriateness of the low-amplitude acoustic model's assumption that the gas displacement amplitude is much smaller than the stack length. The systematic differences between the right and left stacks' disagreements suggest hardware imperfections. However, the shared disagreements suggest a common cause. The peak-to-peak gas displacement amplitude in the stack was 2 cm, of the order of 10% of the length of the stack, so we would not be surprised by 10% errors in results predicted by the low-amplitude thermoacoustic equations, which are based in part on the assumption of negligibly small displacement amplitudes.

Figure 6 shows acoustic power delivered to the resonator from the fronts of the speakers, as a function of steady flow rate. The open circles with error bars represent the measured acoustic power delivered on the left side, found using measured complex pressure amplitudes and the speaker-diaphragm displacement relation given by Eq. (9); the corresponding dark circles are similar values for the right side. The near equality of the left and right results indicates the control achieved by the microphone mixers in balancing the acoustic power delivered to each side of the resonator, but the independence from $\dot{m}$ is a more interesting, less direct consequence of the experimental conditions. The acoustic power delivered to the resonator was independently estimated using an enclosed-speaker algorithm with the measured speaker parameters in the complete numerical model of the apparatus. The circles connected by lines in Fig. 6 represent the values of acoustic power calculated with this numerical model. The numerically estimated acoustic power delivered to the resonator exhibits the same independence of $\dot{m}$ as the measured data, but disagrees in magnitude by almost a factor of 2.

This large disagreement indicates a failure of either or

both of these methods of obtaining $\dot{W}_{ac}$. In hindsight, we suspect that the factory-equipped cooling system built into each speaker causes both methods to be inaccurate for this apparatus. At typical operating conditions, gas velocities induced by the cooling system past the voice coil and through the ports in the magnet were of the order of 50 m/s, and pressure differences of the order of $\rho|u_1|^2/2 \approx 1$ kPa and power dissipations of the order of 10 W per speaker are to be expected in the unstreamlined passages through which this high velocity passed. Neither the numerical model nor Eq. (9) (which assumes that the cavity volume V_{back} experiences spatially uniform oscillating pressure) can account for this complicated situation. Future modeling of such speakers in similar circumstances will require either a more sophisticated analysis than that which led to Eq. (9) here or an effort to choose (or modify) the speakers in order to simplify the cavity geometry.

IV. CONCLUSIONS

Deliberate superposition of steady flow parallel to the thermoacoustic oscillations in a stack can indeed be used to cool the steady flow as it passes through the stack. The agreement between measurements and numerical integrations for stack temperature profile and cooling power summarized in Figs. 4 and 5 suggests that Eq. (4) describes the total power flow in a stack when such steady flow exists.

As $\dot{m}$ was increased, adding steady-flow heat load to the refrigerator, it was necessary to reduce $\dot{Q}_C$ in order to maintain $T_0 - T_C$ constant. Figure 5 shows the details of this tradeoff: The total refrigeration power $\dot{Q}_C + \dot{m}c_p(T_0 - T_C)$ rose with $\dot{m}$. This increase in total cooling power while the acoustic power needed to drive the device remained constant illustrates the increase in efficiency, discussed in the Introduction, that occurs as some of the total heat load is shifted from T_C to temperatures greater than T_C as steady flow increases. If we define the coefficient of performance (COP) as total cooling power divided by acoustic power, the COP increases about 20% as the cooling power is shifted completely from $\dot{Q}_C$ to $\dot{m}c_p(T_0 - T_C)$. This is much less than the ideal factor-of-two efficiency increase discussed in the Introduction, but our refrigerator was also far from ideal in many other respects. At $\dot{m} = 0$, its COP was only roughly 4% of Carnot's COP, and apparently most of the irreversibilities responsible for this low COP are not improved by steady flow. Future exploration of these details will be interesting and important.

Determination of the acoustic power delivered by a speaker based on measurements of complex pressure amplitude on both sides of the speaker diaphragm and knowledge of the enclosed volume on one side requires attention to the details of the enclosed volume, lest pressure differences within the enclosed volume invalidate the theory of the measurement.

This work focused on a standing-wave thermoacoustic refrigerator with parallel superimposed steady flow, but we hope that engines, traveling-wave devices, and devices with perpendicular superimposed steady flow will also demonstrate interesting phenomena and lead to practical applications.

[1] *ASHRAE Handbook: 1995 Applications* (American Society of Heating, Refrigerating, and Air-Conditioning Engineers, Inc., New York, 1995), pp. 9.4–9.6.

[2] A. Bejan, *Advanced Engineering Thermodynamics*, 2nd ed. (Wiley, New York, 1997).

[3] N. Rott, ''Damped and thermally driven acoustic oscillations in wide and narrow tubes,'' Z. Angew. Math. Phys. **20**, 230–243 (1969).

[4] N. Rott, ''Thermally driven acoustic oscillations, Part III: Second-order heat flux,'' Z. Angew. Math. Phys. **26**, 43–49 (1975).

[5] G. W. Swift, ''Thermoacoustic engines,'' J. Acoust. Soc. Am. **84**, 1145–1180 (1988).

[6] R. S. Reid, ''Open cycle thermoacoustics,'' Ph.D. thesis, Georgia Institute of Technology, School of Mechanical Engineering, 1999.

[7] G. W. Swift, ''Thermoacoustics: A unifying perspective for some engines and refrigerators,'' Rough draft available at www.lanl.gov/thermoacoustics/, 1999.

[8] W. C. Ward and G. W. Swift, ''Design environment for low amplitude thermoacoustic engines (DeltaE),'' J. Acoust. Soc. Am. **95**, 3671–3672 (1994). Fully tested software and user's guide available from Energy Science and Technology Software Center, U.S. Department of Energy, Oak Ridge, Tennessee. To review DeltaE's capabilities, visit the Los Alamos thermoacoustics web site at www.lanl.gov/thermoacoustics/. For a beta-test version, contact ww@lanl.gov (Bill Ward) or swift@lanl.gov (Greg Swift) by email.

[9] R. S. Reid, W. C. Ward, and G. W. Swift, ''Cyclic thermodynamics with open flow,'' Phys. Rev. Lett. **80**, 4617–4620 (1998).

[10] G. W. Swift, ''Analysis and performance of a large thermoacoustic engine,'' J. Acoust. Soc. Am. **92**, 1551–1563 (1992).

[11] Endevco, San Juan Capistrano, California 92675, Model 8510B.

[12] Hewlett Packard, Santa Clara, California 95054, Model 35665A.

[13] Omega Engineering, Stamford, Connecticut 06906.

[14] JBL Professional, Northridge, California 91329, Model 2206H/J.

[15] R. S. Wakeland, ''Use of electrodynamic drivers in thermoacoustic refrigerators,'' J. Acoust. Soc. Am. **107**, 827–832 (2000).

[16] T. J. Hofler, ''Accurate acoustic power measurements with a high-intensity driver,'' J. Acoust. Soc. Am. **83**, 777–786 (1988).

[17] S. Ballantine, ''Technique of microphone calibration,'' J. Acoust. Soc. Am. **3**, 319–360 (1932).

[18] A. M. Fusco, W. C. Ward, and G. W. Swift, ''Two-sensor power measurements in lossy ducts,'' J. Acoust. Soc. Am. **91**, 2229–2235 (1992).

[19] Fuji Electric, Tokyo, Japan, blower model 4Z753.

[20] Meriam Instruments, Cleveland, Ohio 44102, Model 50MW20-1 1/2.